Aust. J. Phys., 1986, **39**, 71–92

Experimental Determination of the Imaging Properties of a 200 kV Electron Microscope

S. R. Glanvill, A. F. Moodie, H. J. Whitfield and I. J. Wilson

Division of Chemical Physics, CSIRO, P.O. Box 160, Clayton, Vic. 3168.

Abstract

Optical transforms from a through focal series of images of amorphous films of Ge were used to measure the spatial frequencies of maximum and minimum phase contrast of a specific 200 kV JEOL electron microscope. This information was used to determine precise values for the spherical aberration coefficient and defect of focus. Under the appropriate conditions of lens excitation the spherical aberration coefficient was found to be as low as 0·94 mm. Other image defects revealed with great precision were associated with astigmatism, beam divergence and specimen drift in the microscope stage. Quantitative examples illustrating these effects are discussed.

1. Introduction

Some contemporary electron microscopes can resolve detail on a scale comparable with atomic dimensions. In order to consistently attain this image quality it is vital that a precise understanding of the imaging properties of the microscope under a range of objective lens excitation and illumination conditions be available. Furthermore, for convincing computer-calculated image matching, accurate experimentally determined imaging conditions are required.

Until the advent of electron microscopes with the capability of resolving to better than 3 Å, the accurate determination of electron microscope lens aberration was the province of lens designers rather than electron microscope users. For lattice image calculations it has hitherto been generally satisfactory to determine the spherical aberration coefficient C_s by comparison of calculated and observed images. However, if we wish to interpret the fine detail now observable on high magnification micrographs, then we need to know the precise spherical aberration under the conditions of defect of focus and lens excitation used in obtaining the micrograph.

Thon (1966) has shown that defect of focus and C_s can be determined from the image of a random weak phase object by using an optical Fourier transform processor. The general principles of the process are well known; however, we have found that severe difficulties arise in practice when the accelerating voltage is in the 200 kV range, the Rayleigh resolution is in the vicinity of 2 Å, and the object is to obtain parameters of known accuracy on which to base numerical work. The difficulties derive from the requirement for a good signal-to-noise ratio at high scattering angles

0004-9506/86/010071$02.00

corresponding to spatial frequencies approaching $0{\cdot}5$ Å^{-1}. This is much more severe than it appears from qualitative work. In fact, we have only found it possible to arrive at a satisfactory result by analysing images from specimens of high projected potential in a purpose built optical system having a focal length chosen for compatibility with the image magnification.

For such high projected potentials the weak phase object approximation is no longer valid but, for amorphous materials of simple short range structure, the phase object approximation can be shown to have adequate validity. As a consequence, the images arising from suitable amorphous materials are insensitive in the mean to specimen tilt and thickness. Therefore these parameters need not be controlled in a study of optical performance, a factor which makes it practical to measure microscope behaviour over a wide range of operating conditions. In contrast, lattice images are sensitively dependent on tilt and thickness and the determination of optical parameters by the matching of lattice images is suited only to the determination of discrete values (Lynch *et al.* 1975).

It is the object of this communication to describe detailed procedures for exploring the object image space of the microscope and to obtain electron optical parameters sufficiently accurate to be used in the quantitative numerical analysis of lattice images at 2 Å resolution.

2. Theoretical Details

The use of Fourier optics for the determination of electron optical parameters has proved to be extremely powerful since its introduction by Thon (1966). In its most direct form, which is that used in the present work, images of an amorphous material are analysed with an optical processor to measure the spatial frequency power spectrum.

When simplifying assumptions are made for electron scattering, the parameters which are abstracted are found to be in good agreement with those found from comparison of calculated and experimental lattice images. This agreement has surprising features since, classically, a weak phase object approximation is used in Thon's method whereas a full dynamical treatment is found to be essential in the lattice image analysis. The reasons for this are briefly considered here. In fact, as Kanaya *et al.* (1981) showed, a phase grating approximation can be made in Thon's analysis with no more change than a shift of origin for the defect of focus. The other factors to be taken into account in a full dynamical treatment arise from the kinetic energy terms in the Hamiltonian, appearing as functions of the dynamical excitation errors in the standard solutions. These factors can be shown to be unimportant for simple monatomic glasses consisting of, for instance, carbon, silicon or germanium. A detailed derivation of this result will be the subject of a separate communication but the argument can be outlined in the following way.

The equation describing the forward scattering of electrons in the positive z direction can be written (Goodman and Moodie 1974)

$$\begin{aligned} \mathrm{i}2k\partial\psi/\partial z &= (-2k\sigma\phi - \nabla^2_{xy})\psi \\ &= H\psi, \end{aligned} \tag{1}$$

where ψ is the wavefunction, H is an effective two-dimensional Hamiltonian, k is the

wavevector, $\phi(x, y, z)$ is the scattering potential and

$$\sigma = \frac{\pi}{W\lambda} \frac{2}{1+\{1-(v^2/c^2)\}^{\frac{1}{2}}}, \tag{2}$$

with W the accelerating voltage, λ the wavelength and v the velocity of the electron.

In conventional fashion the differential equation is converted to an integral equation which is solved by iteration to yield

$$\psi = 1 + \mathrm{i} \int_0^T H(z_1)\, \mathrm{d}z_1 + \mathrm{i}^2 \int_0^T \int_0^{z_1} H(z_2) H(z_1)\, \mathrm{d}z_1\, \mathrm{d}z_2 + \ldots, \tag{3}$$

where T is the thickness of the crystal. Omission of the kinetic energy term, that is the differential operator, leads directly to the phase grating approximation. When the atoms are disposed in a monatomic glass, the kinetic and potential energy terms can be shown to anti-commute in the mean to good approximation. The series is then of exponential form with a mean effective phase shift and conventional analysis can be used to determine the electron optical parameters.

3. Electron Optics

A series of high resolution electron images of films of amorphous materials together with a small crystallite, usually of the same material, was taken in the JEOL 200 CX electron microscope. The microscope was used in top entry configuration with an ultra-high resolution objective pole-piece, a double-gap (STEM) pole-piece condenser No. 1 and a polycrystalline LaB_6 electron source. The manufacturer's specification for this objective pole-piece guaranteed a C_s of 1·2 mm or better. Substitution of this value into the standard expression for resolution at the Scherzer focus leads to a value of 2·42 Å. The microscope was carefully aligned at maximum magnification (850 000 nominal) with the sample at a height in the lens characterized at a given magnification by the current used to excite the lens at gaussian focus. Through focus sets of images were taken of the same area of amorphous films of carbon, silicon and germanium at 16 approximately equal steps of defect of focus ranging from +800 to −2400 Å. The stigmator and voltage centring controls were not readjusted during the collection of a through focus series of images.

4. Light Optics

Before describing in detail our experimental arrangements it is useful to consider the scale of operations as it applies to lattice images. The electron image is recorded as a negative on electron sensitive film with a spatial resolution of at least 20 mm^{-1}. For a magnification at the recording plane of 850 000, this spatial frequency corresponds to a specimen structure of 0·6 Å, well below the limit of transferred spatial frequencies of the best electron microscopes. Thus the recording medium, in practice, has sufficient resolution to record faithfully all spatial frequencies likely to be present in an image. However, in the design of the experiment it would be useful to know more precisely the limit of transferred spatial frequency. This limit may be estimated with a knowledge of the beam divergence, chromatic aberration and instrumental stabilities of the electron microscope. Perhaps the best method is to select a value based upon wide experience with a given microscope. Frequently we have observed lattice

images in silicon and germanium crystallites corresponding to the 440 reflections with spacings of 0·9599 and 1·0000 Å respectively. Thus, we believe the limit of transferred spatial frequencies is near 1 $Å^{-1}$ corresponding to about 12 and 14 mm^{-1} at the recording plane with magnifications of 850 000 and 730 000 respectively.

Having established a reasonable spatial frequency bandwidth, we are now able to design the optical Fourier transform processor. The first important design decision to be made concerns the choice of focal length of the optical processor. This is governed by the desire to detect the highest spatial frequency component present in the input transparency on a chosen detector format. There are many obvious advantages to be gained by using Polaroid positive/negative film as a detector. In order to fully utilize the space bandwidth product of the system envisaged, we need to fill almost the entire available detector area (approximately 75×100 mm for Polaroid 665 film). Thus, if for design purposes the highest spatial frequency component of the input transparency is $\eta = 15\ mm^{-1}$ then, in order to diffract this signal to transform plane coordinates within a radius $r = 35$ mm of the zero-order focus, a focal length f such that

$$f = \frac{r}{\eta\lambda} = \frac{35}{15\times 0\cdot 6328\times 10^{-3}} = 3700\ \text{mm} \tag{4}$$

is required. The wavelength λ is taken to be that of the He–Ne laser.

The entrance pupil for the optical processor will be determined by the size of the input transparency. In our case the maximum aperture defined in this way has dimensions 75×100 mm. Rarely is the full aperture used because this generates the familiar Fraunhofer diffraction pattern for a rectangular aperture convoluted with the desired transform. The aperture convolution can be made less intrusive by using a circular aperture or, more conveniently, by underfilling the input transparency with the gaussian illumination of the laser light source. In either case, we find it convenient to use an effective aperture of about 50 mm diameter giving an f number for the system of about 75. This, coupled with the low spatial frequency bandwidth required of the optical processor, suggests that a very simple Fourier transform element will be satisfactory. Indeed a detailed optical design study shows that the simplest system available consists of a single concave mirror working slightly off-axis. This novel configuration has the added advantage of being a compact folded system with adjacent input and output planes.

The actual mirror focal length used in this work was 3805 mm which leads to diffraction limited performance for a 50 mm diameter entrance pupil and design spatial frequency of 15 mm^{-1}. An impression of the geometric image is shown in the spot diagrams of Fig. 1. For reference, the spot size is shown at the focus of a diffraction limited beam that has a gaussian intensity distribution with e^{-2} intensity at a radius of 25 mm in the input plane.

5. Maxima and Minima of the Optical Transform

The effect of the phase contrast transfer function on transferred spatial frequencies can be readily observed with the optical processor described above. As an input, a negative transparency of the electron image of an amorphous specimen is used. The task at hand is to measure the diameter of the transfer function rings at points corresponding to maximum and minimum brightness and then, by means of the

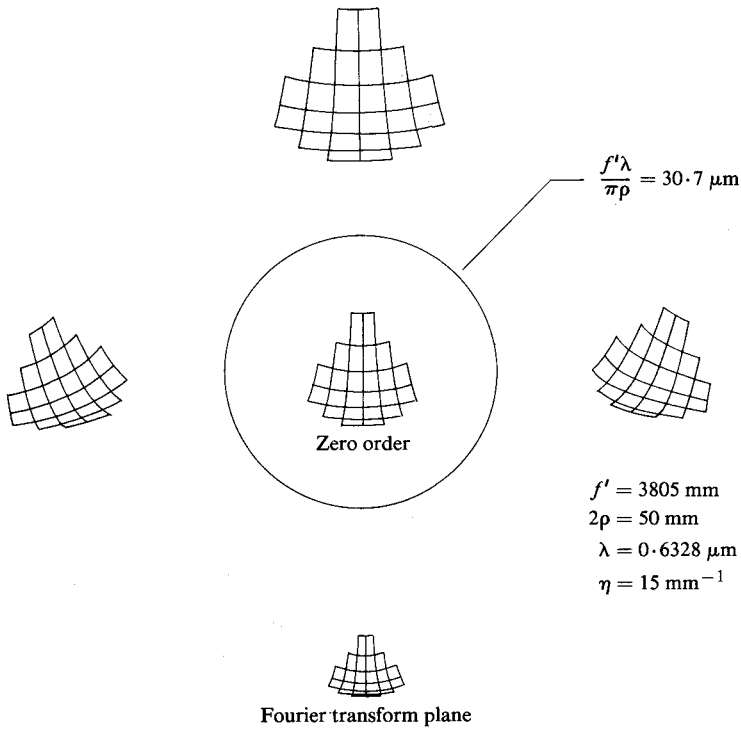

Fig. 1. Spot diagrams showing the geometrical image at the Fourier transform plane for the spatial frequency $\eta = 15\ mm^{-1}$ and wavelength $\lambda = 0{\cdot}6328\ \mu m$.

diffraction spots from a known calibration crystallite, to accurately determine the spatial frequency of these maxima and minima. A useful starting point is the work of Kuzuya and Hibino (1981) concerning the effect of defect of focus on the precision with which the spherical aberration coefficient may be determined. These authors convincingly showed that there is a preferred range of defect of focus values Δf that will lead to optimum precision in the determination of C_s. Following their method, and choosing a tolerance on C_s of $\pm 0{\cdot}025$ mm, we found the range to be approximately $-1000 > \Delta f > -2000$ Å if the spatial frequency of maxima and minima can be determined with an accuracy of about $\delta q_n = \pm 10^{-3}$ Å^{-1}. Here we are at variance with Kuzuya and Hibino (1981) who claimed an accuracy in the determination of spatial frequency of $\pm 2{\cdot}5 \times 10^{-4}$ Å^{-1}. Although this tolerance is quite reasonable for the measurement of the spatial frequency of a discrete spacing such as from a calibration crystallite, it is not reasonable in the measurement of the position of a turning point. In this task there is a certain amount of judgment required, especially for rings far out in reciprocal space where the signal-to-noise ratio is invariably poor. Ironically it is these far out rings that one expects to provide data leading to the highest precision in the determination of C_s. In practice, the tolerance on δq_n begins to diverge with decreasing signal so that there is considerable incentive to try to improve the signal-to-noise ratio of the experiment. These points will be illustrated later in this paper when we give the data corresponding to an actual experiment.

So far we have argued that the presence of noise limits the accuracy with which the spherical aberration coefficient may be determined. Before discussing means for improving the situation, we will consider the main sources of artefact noise. Firstly, there is coherent scattering arising from the random nature of the object and the finite size of the illuminated field. In this case the speckle spot size ρ at the transform plane is approximately given by

$$\rho = 1{\cdot}22f\lambda/2R = 0{\cdot}06\ \text{mm},$$

where $R = 25$ mm is the typical radius of the illuminated field. The speckle density in this case depends in a complicated way on the random object details. Secondly, it is known that a large contribution arises from coherent scattering from the film grain. This is particularly the case with electron sensitive emulsions which are very 'grainy' in the sense of having large silver grains that are easily detected with a low power optical microscope. The film grain Wiener noise spectrum is a maximum around the zero-order focus and depends on the average density D of the input micrograph and the average grain diameter. For example, in a simplified model in which the granular pattern is assumed to be a random array of circular grains of diameter d, the Wiener spectrum can be shown to be

$$F(q,0) = (\pi Dd^2/1{\cdot}72)\{2J_1(\pi qd)/\pi qd\}^2,$$

where $J_1(x)$ is the Bessel function of order 1 and argument x. Consequently, there is much scattering around the zero-order focus, where much of the transfer function information appears. The problem is therefore a fundamental limitation associated with the use of silver halide based electron sensitive film and the need for short exposures, a problem long familiar to electron microscopists.

The inevitable noise present in a given spatial frequency bandwidth appears to be quasi-random. This suggests that signal averaging or smoothing techniques could be useful in improving the signal-to-noise ratio. Perhaps the simplest of these techniques, which we have adopted as standard practice, is to rotate the input transparency about its centroid. Typically the transparency is rotated about 50 times during an exposure so that the noise is smoothed and gives a slowly varying background. To take advantage of the improved signal-to-noise ratio, a background-correction procedure is required where the slope of the background becomes significant. We should stress that it is only valid to adopt the above smoothing procedure when the electron microscope is well adjusted with accurate compensation of astigmatism and with no detectable specimen drift. The optical transform must, in fact, have proper circular symmetry.

The smoothed optical transform is recorded on Polaroid 665 positive/negative film with the scale of operations such that the ring diameters are in the range 10–30 mm. This is ideal for precision measurement by scanning the negative with a microdensitometer. The measurement errors associated with a microdensitometer are insignificant compared with the ability to judge the turning points of the transform. Another advantage stems from the ability to effect a further improvement in signal-to-noise ratio. The slit height is measured perpendicular to the scanning diameter, i.e. tangentially to the rings, and consequently can be chosen to be considerably greater (1–2 mm) than the slit width (0·1 mm). The improvement in signal quality obtained by this procedure is illustrated in Fig. 2 which shows the results of raw data and those after smoothing. The microdensitometer settings were the same for each scan.

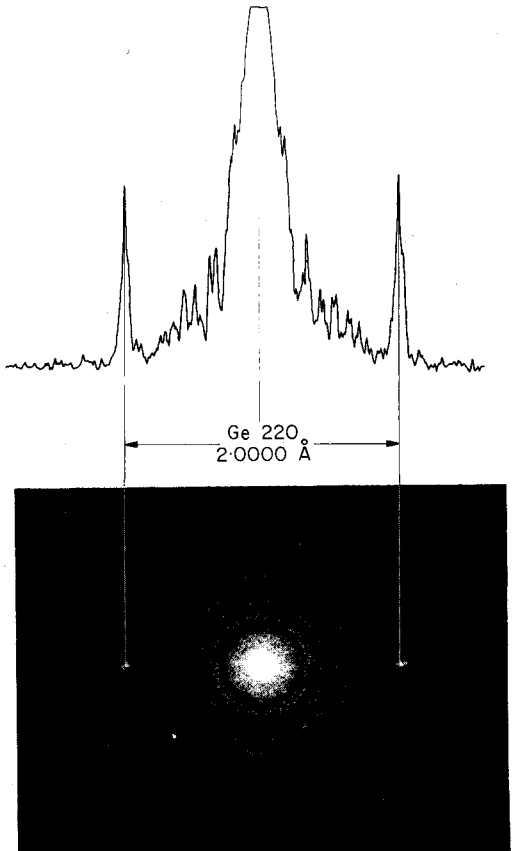

Plate 16791

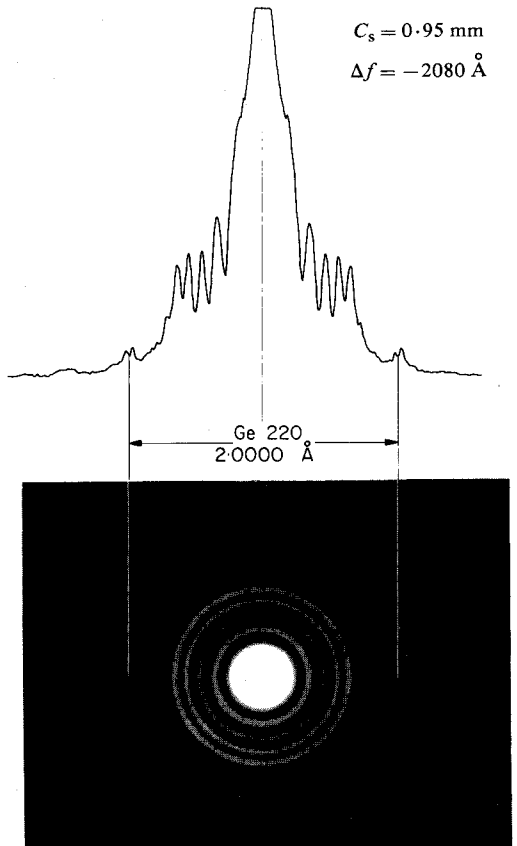

Plate 16791

Fig. 2. Optical transforms obtained with the input micrograph stationary and following rotation. Accompanying micro-densitometer traces clearly show significant noise reduction from rotation smoothing.

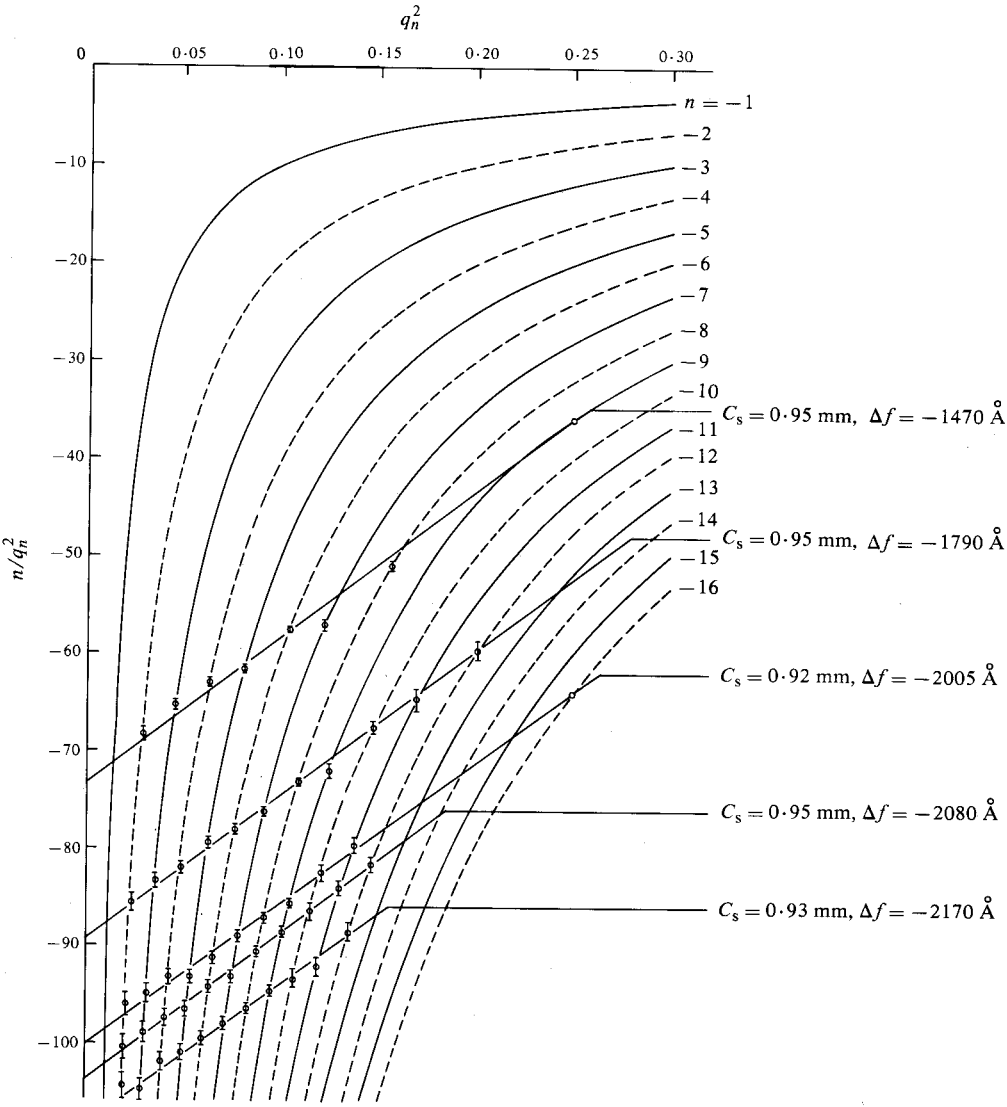

Fig. 3. Experimental results from a through focal series used to derive values of C_s and Δf by following the method of Krivanek (1976).

6. Spherical Aberration

Following preliminary inspection for poor astigmatism setting and specimen drift, the micrographs of a through focus series were processed as described in the previous section. The turning points q_n and an error estimate δq_n were determined from the spatial frequency power spectrum and a graph of n/q_n^2 against q_n^2 was plotted by following the method of Krivanek (1976). The data should fall on a straight line with slope $C_s \lambda^3$ and intercept $2\Delta f \lambda$. Fig. 3 shows the results obtained from selected micrographs of a through focal series for objective lens excitation of 6·20 A. This

value may be compared with the commonly used value of 5·80 A and corresponds to an estimated change in focal length of 5%. Included in the data set are two extra results plotted for $q_n^2 = 0{\cdot}25$ and $\Delta f = -1470$ and -2005 Å. These points are fortuitous results derived from observations of the intensity of the diffracted orders corresponding to the Ge 220 calibration crystallite. In the first case, the intensity of the Ge 220 diffracted orders appears to be a maximum for $\Delta f = -1470$ Å. In the second case, the intensity of the Ge 220 diffracted orders is extinguished at $\Delta f = -2005$ Å. Data obtained in this way are particularly valuable since they accurately establish the spatial frequencies of maximum and minimum contrast in a remote region of reciprocal space where the scattering amplitude arising from the amorphous component is quite small and not detected in our experiment. In this region we have also found crystallites of gold and silicon to be quite useful in furnishing discrete data points, particularly when the optical transform shows the disappearance of the calibration spots for one defect of focus.

A typical data set for five different defects of focus in the preferred range $-1000 > \Delta f > -2500$ Å is used to provide an average slope and then, with a knowledge of the electron wavelength, the value of C_s for a given lens excitation is obtained. It is worth noting that the electron wavelength should be known accurately since small errors strongly influence the resulting value of C_s. In particular, when $C_s = 1$ mm, $\lambda = 0{\cdot}025$ Å and $\delta\lambda = 0{\cdot}0001$ Å, the change in C_s is

$$\delta C_s = 3\delta\lambda C_s/\lambda = 0{\cdot}01 \text{ mm}. \tag{5}$$

For the electron microscope used in this work, the electron wavelength measured by the method of Kikuchi lines was found to be (Fitzgerald and Johnson 1984)

$$\lambda = 0{\cdot}02509 \pm 0{\cdot}00001 \text{ Å}.$$

The average slope for the data of Fig. 3 was found to be 148·17, giving a value for C_s of 0·938 mm. The value of C_s determined for individual defects of focus is shown in Fig. 3 and gives some indication of the precision of the experiment. Measured values of C_s ranging from 0·92 to 0·95 mm are consistent with our expected tolerance on C_s of $\pm 0{\cdot}025$ mm, based on the work of Kuzuya and Hibino (1981). These values derive from an objective lens excitation of 6·20 A, a current appropriate to the object distance at which our tilt holders have been set. A value of 1·14 mm was obtained for fixed holders where the object distance is greater and the corresponding current is 5·9 A.

It is worth noting that powerful evidence supporting our experimentally determined value of C_s has been obtained from multi-slice image matching calculations. For a lens excitation similar to that used in our experiment, a C_s value in the range 0·90–0·96 mm is required to provide a high fidelity image match.

7. Defect of Focus and Microscope Calibration

Having established an accurate value for the spherical aberration coefficient for a given lens excitation, we can then readily determine the defect of focus over the useful operating range of the microscope. In particular, for defect of focus values less than -1000 Å there are usually only one or two rings in the optical transform

with which to measure the defect of focus. Following the method of Kuzuya and Hibino (1981), the defect of focus is obtained by choosing a line of best fit with a slope that is consistent with the previously determined value of C_s. In this way the focus adjustment of the microscope is calibrated. We give an example in Fig. 4 for the JEOL 200 CX microscope that was used in this work. The ordinate is expressed in clicks of the second finest focusing knob. The data show a linear change of defect of focus with focusing increment and the slope indicates a change of focus of about 400 Å per click. It is of interest to note that the operator selected the defect of focus corresponding to minimum image contrast as the reference defect of focus and nominally called this the gaussian focus. However, the results in Fig. 4 show that, in fact, the condition of minimum contrast in this case corresponds to a defect of focus of about -180 Å. To a first approximation this result may be understood in terms of a convolution of the microscope transfer function for slightly negative defect of focus and the specimen scattering envelope. The dominant feature of the transfer function is the influence of the nearby $n = 0$ minimum causing very low image contrast except for a small band of spatial frequencies passed by the $n = +1$ maximum. At the gaussian focus the transfer function has a higher response and hence more image contrast until the $n = +2$ minimum is encountered near spatial frequency $0{\cdot}33$ Å^{-1}. In addition, departure from the first Born approximation manifests itself as a small effective phase shift which also leads to a change of origin as reported by Kanaya *et al.* (1981), and referred to in Section 2.

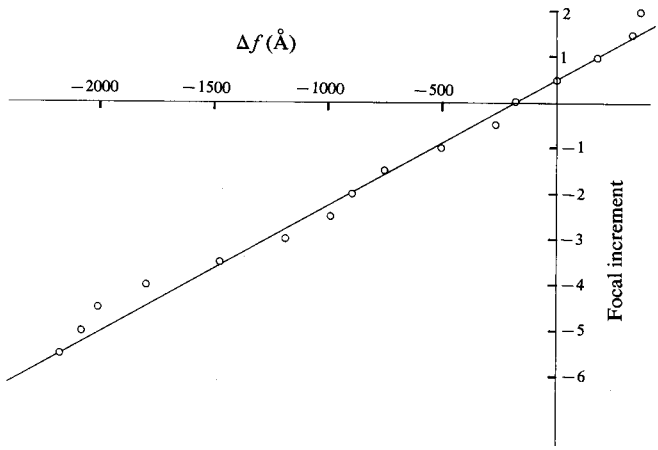

Fig. 4. Calibration of the JEOL 200 CX microscope showing focal increment against Δf.

8. Astigmatism

Primary astigmatism is an azimuthally dependent focusing effect causing the sagittal and tangential focal surfaces to be axially displaced. It is convenient to quantify astigmatism in terms of the displacement C_a known as the astigmatic difference or simply the astigmatism coefficient. The phase change due to primary astigmatism on the back focal plane of the objective lens is given by

$$\exp\{(2\pi i/\lambda) C_a q^2 \lambda^2 \cos 2\phi\}.$$

The transfer function is then proportional to

$$\exp\{i\chi(q)\} = \exp[(2\pi i/\lambda)\{\tfrac{1}{4}C_s q^4\lambda^3 + \tfrac{1}{2}q^2\lambda(\Delta f + \tfrac{1}{2}C_a \cos 2\phi)\}], \quad (6)$$

where ϕ is the scattering azimuth angle. In a well-adjusted microscope the sagittal ($\phi = 0$) and tangential ($\phi = \frac{1}{2}\pi$) focal surfaces are brought into axial coincidence by proper use of the stigmator controls thereby realizing stigmatic imaging conditions with $C_a = 0$. There will then be no azimuthal variation of focus and the optical transform will have the form of the now familiar concentric ring pattern. If a small amount of astigmatism is present the ring pattern will distort, initially to a set of ellipse-like figures. The major and minor axes of a given figure correspond to the extremes of spatial frequency associated with the particular astigmatic difference. We can express this mathematically as follows. The spatial frequency q_n of the maxima and minima in the optical transform correspond to solutions of

$$\chi(q) = \tfrac{1}{4}C_s q^4\lambda^3 + \tfrac{1}{2}q^2\lambda(\Delta f + \tfrac{1}{2}C_a \cos 2\phi) = \tfrac{1}{4}n, \quad (7)$$

where n is zero or an $\pm$integer. If we put

$$\Delta f + \tfrac{1}{2}C_a \cos 2\phi = \Delta F, \quad (8)$$

the solutions are

$$q_n^2 = [-\tfrac{1}{2}\Delta F\lambda \pm \{(\tfrac{1}{2}\Delta F\lambda)^2 + \tfrac{1}{4}nC_s\lambda^3\}^{\frac{1}{2}}]/\tfrac{1}{2}C_s\lambda^3. \quad (9)$$

We note that this expression implies that, for a small degree of astigmatism and relatively large positive or negative defect of focus, $q_n(\phi)$ is approximately constant for a given n. In other words, the optical transform, to a good approximation, takes the form of the stigmatic case. On the other hand, high sensitivity to astigmatism is observed in the optical transform near the optimum defect of focus for a given n. This defect of focus can be found in a straightforward manner by solving the equations

$$\chi(q) = \tfrac{1}{4}C_s\lambda^3 q^4 + \tfrac{1}{2}\Delta f\lambda q^2 = \tfrac{1}{4}n \quad (10)$$

$$d\chi(q)/dq = 0, \quad (11)$$

to give

$$\Delta f = (nC_s\lambda)^{\frac{1}{2}}, \quad (12)$$

$$q_n^2 = (-n/C_s\lambda^3)^{\frac{1}{2}}. \quad (13)$$

At some defects of focus the sensitivity of the transform to astigmatism is much greater than at others. It is therefore possible to mistakenly infer that the astigmatism is changing with defect of focus. As the above discussion shows, this need not be the case. We can illustrate this by reference to selected micrographs from a through focal series (Fig. 5). The astigmatism coefficient is estimated to have a low value

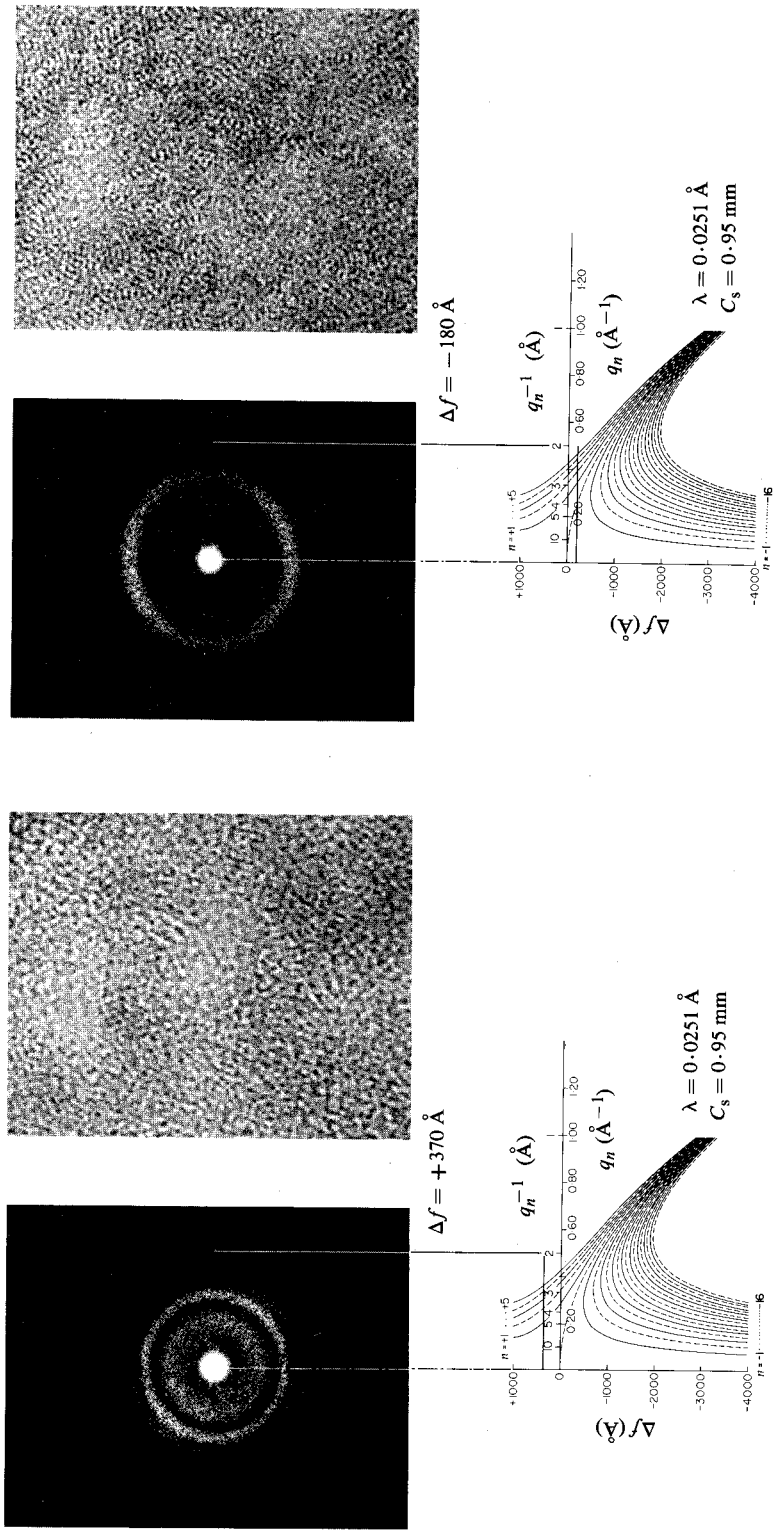

Fig. 5. Optical transforms from a micrograph of an amorphous germanium film with mean Δf as shown.

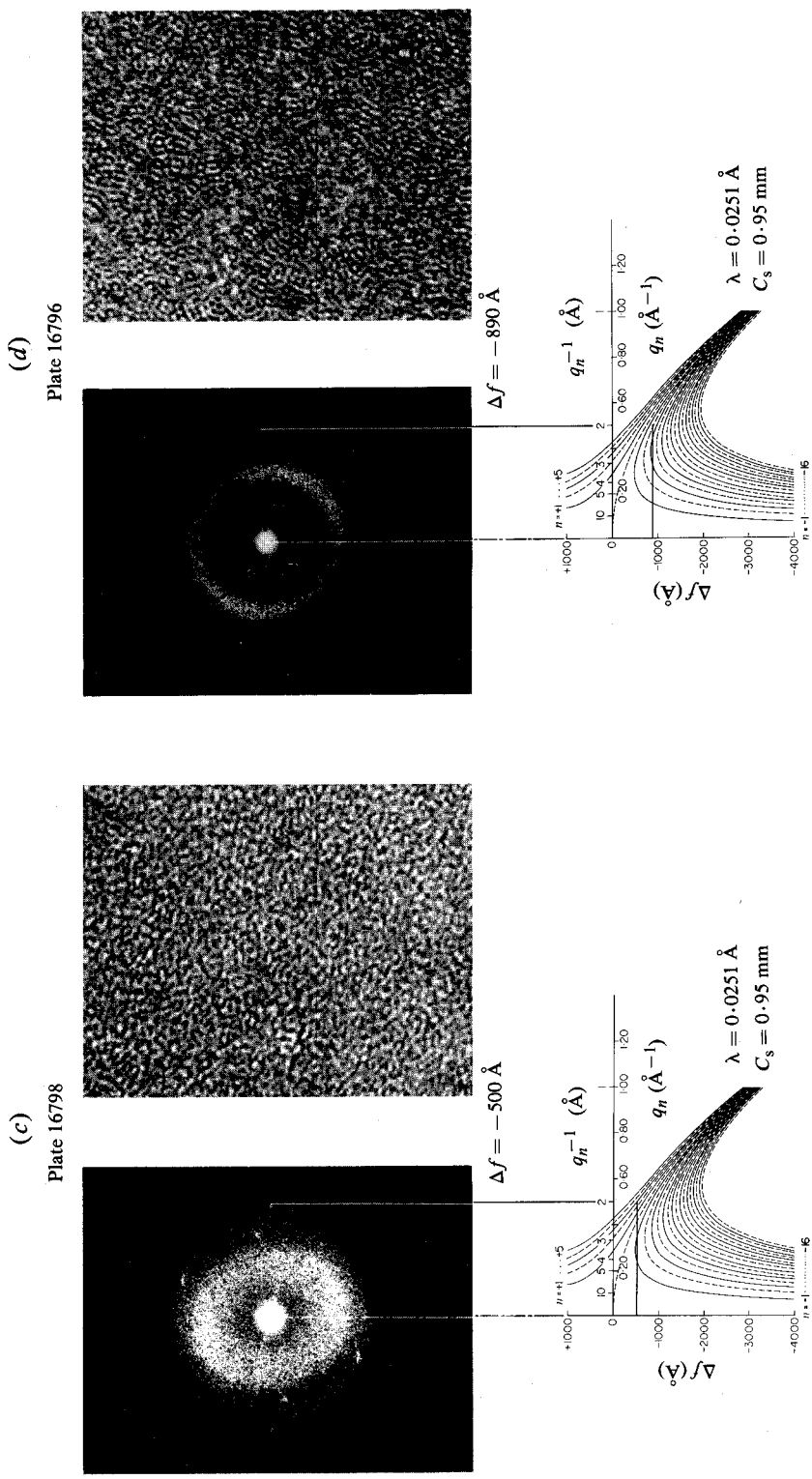

Fig. 5. *(Continued)*

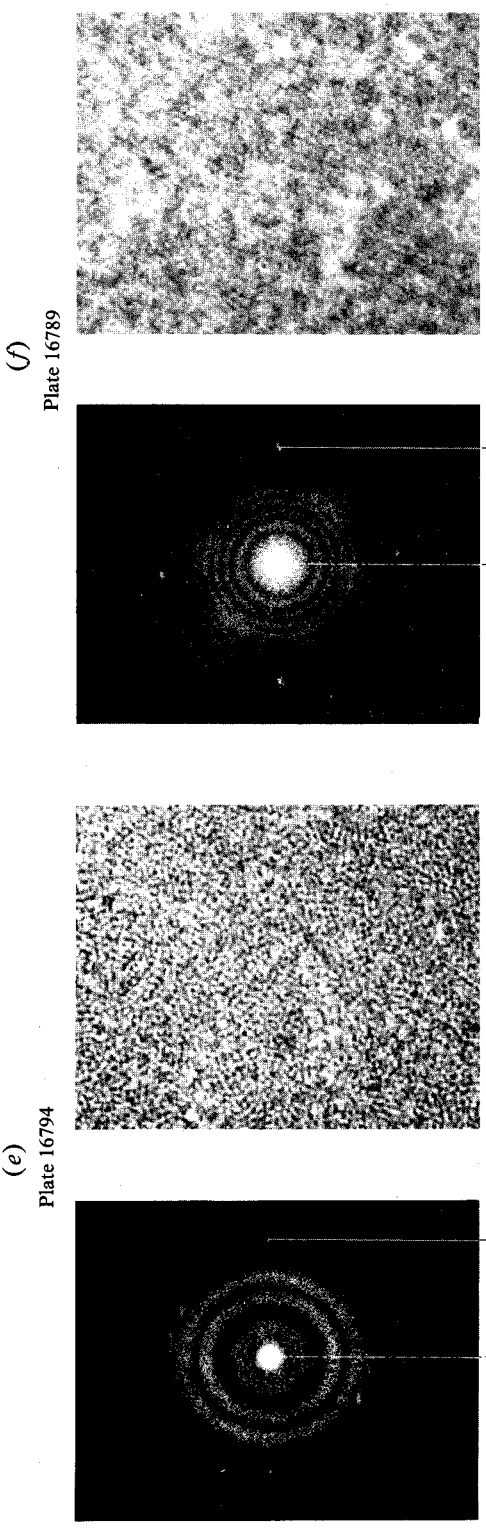

Fig. 5. *(Continued)*

of 50 Å. The presence of this amount of astigmatism is not apparent in the optical transforms for a large defect of focus (Fig. 5*f*) but becomes clear near the optimum focus for $n = -1$ in Figs 5*c* and 5*d*. Also shown in Fig. 5 is the mean defect of focus, indicated as a horizontal line on the accompanying graph of the solution set $\chi(q) = \frac{1}{4}n$. The spatial frequency scale of the graph is the same as for the accompanying optical transform image.

If the experimental conditions permit observable scattering in the optical transform for spatial frequencies

$$q^2 > (n/C_s\lambda^3)^{\frac{1}{2}}$$

then new effects become apparent. In this situation both solutions for q_n^2 in equation (9) may be observed as two or more figures having orthogonal symmetry axes. A simple example of this occurs in Fig. 5*c* where the ellipse-like figures having orthogonal major axes can be seen. Of further interest in this case are the points where the major and minor axes of the figures touch. This is the special solution to equation (9) when the discriminant is zero. Then q_n^2 is single-valued such that

$$q_n^2 = -\Delta F/C_s\lambda^2 . \tag{14}$$

A useful consequence of this special solution is the simple relationship between C_a and the other parameters. If C_s is fairly well known then q_n and ϕ corresponding to the above solution can be measured from the optical transform. Then a value for ΔF can be determined and, with a knowledge of Δf and measured ϕ, the astigmatism coefficient can be determined from equation (8).

When severe astigmatism is present the optical transform becomes much more complicated. For large defects of focus the optical transform shows a family of ellipse-like figures as in Fig. 6. However, for some moderate defects of focus, the second solution of equation (9) becomes real and can be observed. Usually only part of the transform figure is apparent because of the low scattering at the high spatial frequencies involved. Nevertheless it is possible to see some of the interesting features such as the points where the discriminant becomes zero and then positive leading to real solutions to equation (9). In this case we see a branch point in the optical transform as the positive and negative solutions to equation (9) move off through reciprocal space along different trajectories having reflection symmetry about two orthogonal axes. Good examples of these effects can be seen in the through focal series of Fig. 6.

An attempt was made to compute theoretical counterparts to the above through focal series based on solutions to equation (9) and by assuming that the astigmatism coefficient C_a was constant. It was found that, although the basic features of the optical transform could be matched for individual micrographs, it was not possible to achieve a convincing result for the complete series. It was clear that our tentative assumption of the constancy of astigmatism was not justified. There are good grounds for not expecting the astigmatism to be constant with defocus since the stigmator pole-pieces are far removed from the specimen plane of the microscope objective lens in the case of the JEOL 200 CX microscope. It is rather a tribute to the sensitivity of the Fourier optics approach adopted here that the subtle second-order effects due to changes in astigmatism can be observed. The theoretical match to the

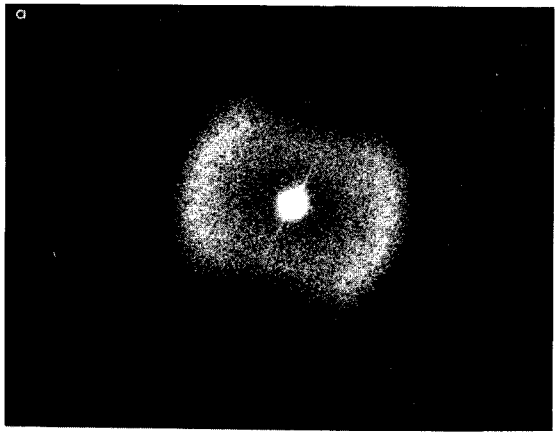

Plate 16774

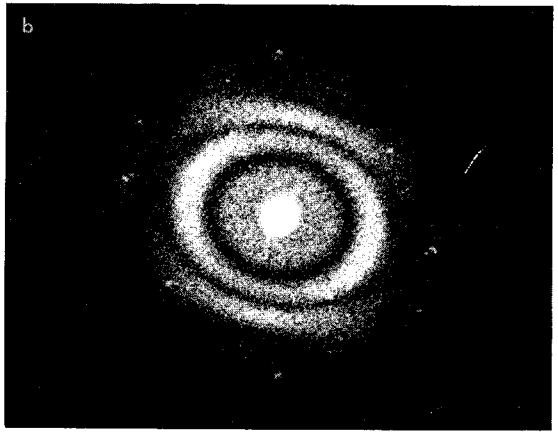

Plate 16771

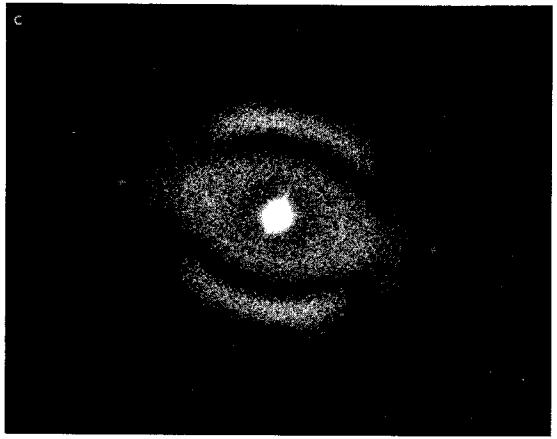

Plate 16773

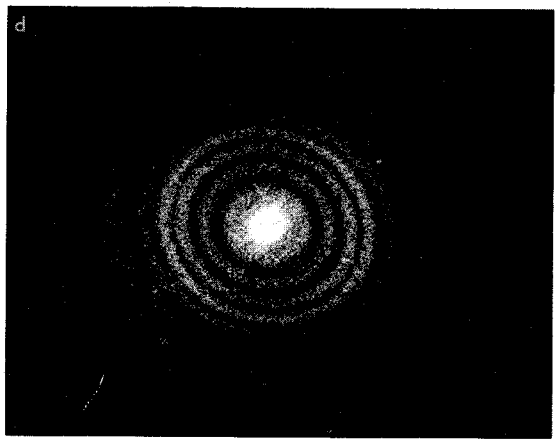

Plate 16767

Fig. 6. Optical transforms from a through focal series showing severe astigmatism resulting from incorrect stigmator adjustment.

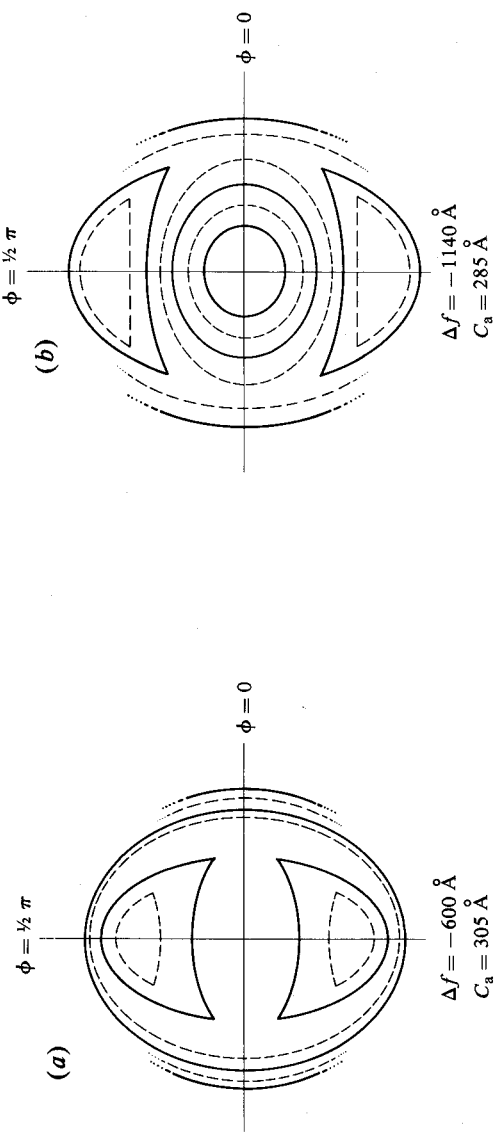

Fig. 7. Calculated reciprocal space trajectories of transfer function maxima (solid curves) and minima (dashed curves) fitted to the corresponding experimental results in Figs 6*a–d*.

results in Fig. 6 is presented in Fig. 7 and shows that the astigmatism coefficient changes approximately linearly from 305 to 240 Å when the defect of focus is changed from −600 to −1740 Å. A detailed theoretical study of the electron optics is beyond the scope of this paper, the authors being content to demonstrate experimentally that astigmatism can change with defect of focus.

9. Other Image Defects

We complete our discussion of the imaging properties of the electron microscope by briefly illustrating how the Fourier optics approach, adopted throughout this work, may be used to reveal the effects of beam divergence and specimen movement.

The effect of beam divergence on the microscope transfer function is that of an envelope function that exponentially damps the high frequency response of the instrument. Proper adjustment of beam divergence is therefore critical in achieving ultimate microscope lattice resolution. To illustrate this point we show in Fig. 8 optical transforms derived from two micrographs of the same field of view and defect of focus having beam divergence β estimated as 5×10^{-4} and 10^{-4} rad. In the former case the optical transform shows the strong 220 reflection from the germanium calibration crystallite and no other finer spacings. However, when the beam divergence is reduced to 10^{-4} rad the 220 reflections considerably increase in intensity while other new reflections corresponding to very fine lattice spacings appear. In particular, the presence of lattice fringes corresponding to the 222 and 422 reflections of germanium at 1·633 and 1·155 Å can be observed both in the direct image and clearly in the optical transform of Fig. 8.

Specimen movement is not an electron optical effect. However, at times its presence can have the appearance of astigmatism both in the direct image and in the optical transform. The image and resulting optical transform resulting from specimen movement are well understood in terms of the theory of linear motion blurring. In the field of electron microscopy this problem has been adequately treated by Frank (1969) and is beyond the scope of the present work. We merely state the main consequence which is to cause the intensity of the optical transform to be modulated by an envelope function. The most common form of specimen movement is a slow uniform drift causing the image to move across the film plane during exposure. In this case the envelope function is

$$\{\sin(\pi k\Delta r)/\pi k\Delta r\}^2,$$

where k is the spatial frequency measured in the direction of drift and $\Delta r = vT$ is the total distance moved after an exposure time T at drift velocity v. In Fig. 9 we show a remarkable example of this type of drift where gross movement in the vertical direction is quite clear in the direct image. Fortuitously the calibration crystallite has the 220 lattice fringe aligned with the direction of motion so that precise calibration of the optical transform is still possible. This enabled the spatial frequency of the first zero in the envelope function to be measured accurately, thereby yielding a solution for the total drift of $\Delta r = 6{\cdot}6$ Å. The exposure time was 4 s giving a drift velocity of 1·65 Å s^{-1}.

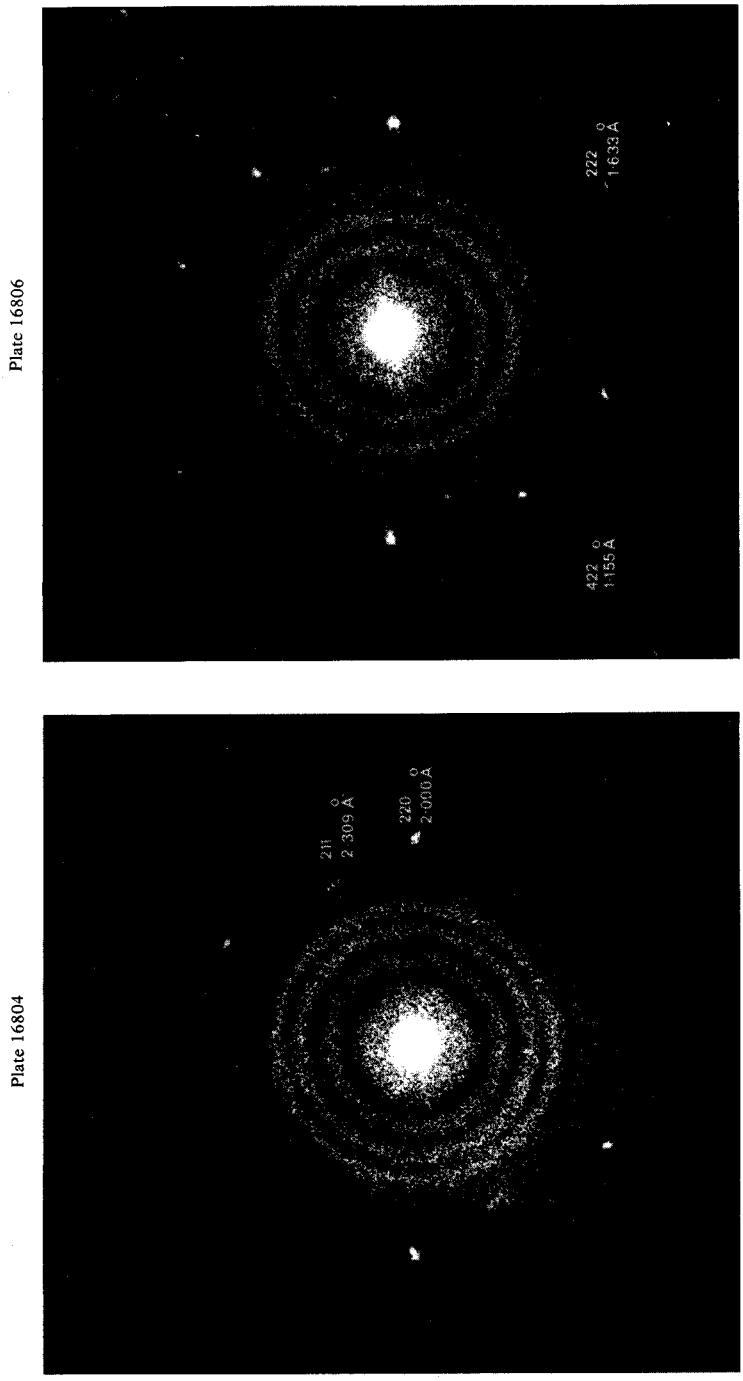

Fig. 8. Optical transforms showing how reduced beam divergence has improved lattice fringe resolution.

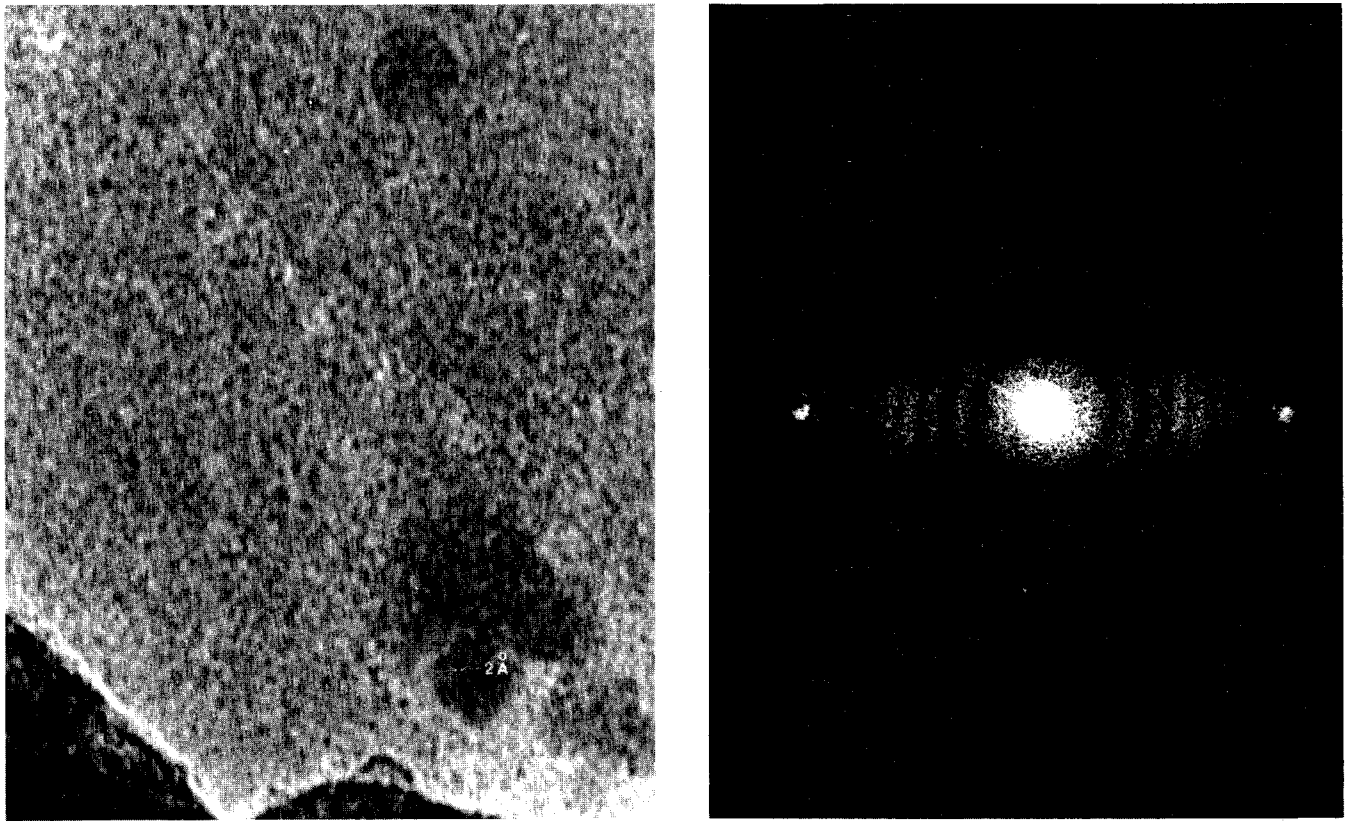

Fig. 9. Image blurring due to uniform linear motion of the specimen. Analysis of the optical transform envelope function reveals a drift velocity of $1{\cdot}65$ Å s^{-1}.

10. Preparation of Amorphous Films

Amorphous films of carbon, silicon and germanium were prepared by sublimation at pressures ranging from 4×10^{-4} to 2×10^{-5} Pa. The films were prepared in a conventional bell jar evacuated by a 400 L s^{-1} diffusion pump backed by a 200 L min^{-1} rotary-vane oil pump. The chamber was routinely vented with dry nitrogen for these experiments. The films were stripped with twice-distilled water and supported on either No. 1500 mesh grids or on holey carbon support films (Glanvill 1980). Germanium and silicon films were deposited at a rate of approximately 40 nm min^{-1} onto substrates of cleaved rocksalt at 20°C. Carbon was rapidly deposited onto a glass substrate, also at 20°C. Germanium was evaporated from a seven-turn tungsten-basket onto a target at a distance of 10 cm. A procedure was developed for the evaporation of silicon, that overcomes the rapid alloying process with tungsten, by preparing tungsten carbide baskets. Tungsten baskets (seven-turn) heated to red heat were reacted with carbon vapour at a pressure between 10^{-3} and 10^{-2} Pa. The performance of these baskets was such that up to four evaporations of silicon could be performed from each basket. The films of silicon and germanium, although having a generally amorphous structure, displayed a large number of microcrystallites scattered throughout the film. There was evidence of occasional graphitization of the carbon films.

11. Conclusions

The two most important imaging conditions quantify the defect of focus and spherical aberration coefficient. Although in principle these quantities are readily obtained from the phase contrast transfer function measured with an optical Fourier transform processor, it is apparent that this is rarely done in practice. Many of the previous experiments have been performed with amorphous carbon films, however, our work shows that this material is not suitable for precise determination of the low value of the spherical aberration coefficient associated with the best microscopes and particularly at voltages of 200 kV or higher. Amorphous silicon films result in some improvement while amorphous germanium films lead to the accurate characterization of the microscope transfer function and hence the spherical aberration coefficient and defect of focus. The lowest value for spherical aberration measured for our particular configuration of the JEOL 200 CX microscope at a lens excitation of 6·2 A was 0·94 mm. If this value is substituted into the standard expression for resolution at the Scherzer focus a value of 2·27 Å is obtained.

Other image defects revealed with great sensitivity by means of the optical processor include the presence of astigmatism, movement of the sample and divergence of the beam. In the experiments with this particular instrument no effects were detected due to misalignment of the illumination (Smith *et al.* 1983), and this result is reinforced by the match with lattice image calculations on known crystal structures.

Acknowledgment

The authors thank Dr C. J. Mitchell, CSIRO Division of Chemical Physics, for providing the spot diagram shown in Fig. 1.

References

Fitzgerald, J. D., and Johnson, A. W. S. (1984). *Ultramicroscopy* **12**, 231.
Frank, J. (1969). *Optik (Stuttgart)* **30**, 171.
Glanvill, S. R. (1980). *Micron* **11**, 355.
Goodman, P., and Moodie, A. F. (1974). *Acta Crystallogr.* A **30**, 280.
Kanaya, K., Kihara, H., and Ishigaki, F. (1981). *Micron* **12**, 105.
Krivanek, O. L. (1976). *Optik* **45**, 97.
Kuzuya, M., and Hibino, M. (1981). *J. Electron Microsc.* **30**, 114.
Lynch, D. F., Moodie, A. F., and O'Keefe, M. A. (1975). *Acta Crystallogr.* A **31**, 300.
Smith, D. J., Saxton, W. O., O'Keefe, M. A., Wood, G. J., and Stobbs, W. M. (1983). *Ultramicroscopy* **11**, 262.
Thon, F. (1966). *Z. Naturforsch.* **21a**, 476.

Manuscript received 30 May, accepted 24 September 1985